HIGH PERFORMANCE PLA/GO POROUS NANOFIBER MEMBRANES
Preparation Strategies and Performance Exploration

by

Jianming WANG[a], Ya CHEN[b], Lei ZHAO[a,c,d*], Jumei ZHAO[a], Kuikui ZONG[e], Chunxia WANG[f], Chunqin MA[g], and Qihu BU[g]

[a] Textile and Clothing College, Yancheng Polytechnic College, Yancheng, China
[b] College of Materials Science and Engineering, Yancheng Institute of Technology, Yancheng, China
[c] College of Textile and Clothing Engineering, Soochow University, Suzhou, China
[d] Institute of Flexible Functional Materials, Yancheng Institute of Technology, Yancheng, China
[e] Suzhou Jingfei Textile Technology Co., Ltd, Suzhou, China
[f] College of Textile and Clothing, Yancheng Institute of Technology, Yancheng, China
[g] Jiangsu Yueda Textile Group Co., Ltd, Yancheng, China

Original scientific paper
https://doi.org/10.2298/TSCI2602203W

In this study, a comprehensive experimental design was employed to investigate the impact of four key factors on the spinning of polylactic acid (PLA) nanofibers. The four factors, namely the solute concentration of PLA, the solvent ratio, the spinning voltage, and the spinning receiving distance, were meticulously optimized through an L9(34) orthogonal experiment. The determination of the optimal process parameters for the preparation of PLA porous nanofiber membranes was achieved through the utilization of SEM and the analysis of fiber diameter data. The polymeric liquid adhesive was concentrated to 8 wt.%, the solvent ratio (DCM:DMF) was set at 9:1, the spinning voltage was set at 20 kV, and the spinning distance was set at 18 cm. In light of these findings, a series of PLA/GO porous nanofiber membranes with varying concentrations of graphene oxide (GO) were meticulously prepared. The study examined the impact of different GO contents on the properties of the fibers. The experimental approach entailed the assessment of several parameters, including surface energy measurement and thermogravimetric analysis. The results demonstrated that when the GO concentration was set at 0.5 wt.%, the PLA/GO porous nanofiber membrane with uniform diameter distribution.

Key words: *electrospinning, nanofiber, porous structure, GO, performance*

Introduction

Electrospinning is a process that can be used to prepare a wide variety of polymers into nanofibers, with different morphologies, including porous fibers, non-smooth fibers, and beaded fibers, among others [1-4]. A plethora of methodologies have been developed for the fabrication of porous materials. These include the sol-gel method and the hydrothermal synthesis method, which are frequently employed [5, 6]. A select group of researchers have also employed the precipitation method, the template method, and the phase transition method, among others. However, the majority of these methods are unsuccessful in the preparation of porous nanofibers. Conversely, electrospinning has been shown to be an effective method for

* Corresponding author, e-mail: zhaolei7365@163.com

the production of porous nanofibers through the mechanisms of liquid phase separation and solid phase separation pore-forming methods [7-9]. The merits of electrospun porous nanofibers are twofold: their high specific surface area and their high porosity. Consequently, there is considerable potential for in-depth exploration in various fields, including materials science, chemistry, cell biology, and MEMS systems [10-12].

The PLA is an environmentally friendly polymer material that can be extracted from plants. It is biodegradable and can be converted into CO_2 and water, and can be recycled repeatedly [13-17]. The PLA is biocompatible and can become part of tissues and systems. The PLA is characterized by its ease of processing and its ability to assume diverse forms, making it a versatile material in a wide range of applications, including adsorption, biomedical engineering, catalysis, sensors, and related fields. The PLA is a biodegradable polymer that has the capacity to completely absorb heavy metals and dyes within a predetermined time range.

Despite its recognized hydrophobic characteristics and favorable mechanical properties, PLA exhibits suboptimal toughness. The GO, due to its abundant functional groups, exhibits greater activity than graphite. The material exhibits notable hydrophilicity, attributable to the presence of a substantial number of hydroxyl and carbonyl groups, a considerable specific surface area characterized by a layered structure, and exceptional mechanical properties. Consequently, the amalgamation of PLA and GO in the fabrication of composite nanomaterials enables the optimal exploitation of the advantages inherent in this material. The present study is predicated on the utilization of spiral electrospinning technology. Firstly, the optimal process parameters for preparing pure PLA porous nanofibers are obtained through orthogonal experiments. It is evident that the utilization of PLA and GO, two environmentally friendly materials that are devoid of any pollution, in a compounding process results in the preparation of PLA/GO porous nanofibers.

Materials and preparation

The materials and chemical reagents primarily utilized in the experiment are enumerated in tab. 1. All reagents utilized in this study are of analytical grade and have not undergone any purification processes.

The instruments and equipment utilized in the experiment are enumerated in tab. 2. Furthermore, 30 mL and 50 mL brown reagent bottles, disposable sterilized syringes (10 mL), weighing paper, aluminum foil, sealing glue, self-sealing bags, and other assorted materials were utilized in the experiment.

Table 1. Materials and reagents

Experimental materials and reagents	Basic information	Manufacturer
PLA	M_w = 100000	Shenzhen Guanghua Weiye Co., Ltd.
GO		Suzhou Gree Pharmaceutical Technology Co., Ltd.
Deionized water	Inspire s200	Shanghai Yudong Water Treatment Co., Ltd.
N-N-dimethylformamide (DMF)	M_w = 73.09	Shanghai Chemical Reagent Co., Ltd.
Dichloromethane (DCM)	M_w = 84.93	Shanghai Chemical Reagent Co., Ltd.

As indicated in tab. 3, prepare spinning solutions with nine distinct solute concentrations and solvent ratios, with 10 g of each solution prepared. In order to prevent rapid solvent evaporation and changes in solution concentration, which may affect the quality of the spin-

ning process, it is essential to adhere to the principle of preparing and using the solution immediately. Due to the low concentration of PLA solute, it is difficult to stretch into fibers during the spinning process. Consequently, the solute concentration utilized in this study commences at 8 wt.%. Concurrently, the high solute concentration of the final solution will render it too viscous to be stretched into fibers. Consequently, the maximum solute concentration permitted in the spinning solution is 10 wt.%.

Table 2. Experiment instrument

Experimental instruments	Model	Manufacturer
Constant flow injection pump	ISP01-A	Baoding Lange Constant Flow Pump Co., Ltd.
High voltage electrostatic generator	DW-P403-1ACCC	Dongwen High Voltage Power Supply Co., Ltd.
Ultrasonic cleaning machine	SL-5200DT	Nanjing Shunliu Instrument Co., Ltd.
Electronic balance	CP214	Ohus Instruments Co., Ltd.
Electric constant temperature drying oven	DHG-924A	Shanghai Pudong Rongfeng Scientific Instrument Co., Ltd.
Magnetic stirrer	HJ-6A	Gongyi Yuhua Instrument Co., Ltd.
Cold field SEM	S-4800	HITACNT, Japan
Simultaneous thermal analyzer (TGA/DSC)	Q600	TA Instruments, America

Table 3. Preparation of PLA fiber membrane by orthogonal test

Test number	PLA solute concentration [wt.%] - A	Solvent ratio (DMC:DMF) - B	Spinning voltage [kV] - C	Spinning receiving distance [cm] - D
1	8	7:3	16	15
2	8	8:2	18	18
3	8	9:1	20	21
4	9	7:3	18	21
5	9	8:2	20	15
6	9	9:1	16	18
7	10	7:3	20	18
8	10	8:2	16	21
9	10	9:1	18	15

In this study, the primary factors examined were the PLA solute concentration, solvent composition, spinning voltage, and spinning receiving distance. The experimental design employed for the preparation of the fibers was a four-factor, three-level L9(34) orthogonal design. The prepared spinning solution was then injected into a 10 mL disposable syringe, and the spinning flow rate was set at 1 mL per hour. The experimental environment was maintained at a temperature of 25 ±1 °C and a humidity level of 55 ±1%. The experimenter may control the temperature and humidity using a humidifier and a heating device.

In accordance with the optimal process parameters for the solute and solvent of pure PLA, varying proportions of GO (GO: 0.1 wt.%, 0.2 wt.%, 0.5 wt.%, and 1.0 wt.%) are incor-

porated into DMF. Following a two-hour oscillation in an ultrasonic bath, 8 wt.% of PLA and DCM are introduced into the mixture. The solvent ratio is DCM:DMF = 9:1. The mixture is stirred at room temperature for a period of six hours, and subsequently sonicated for a duration of half an hour prior to spinning. The prepared spinning solutions are all contained in brown, wide-mouth bottles to prevent DCM photocatalysis. It is imperative to exercise caution with regard to the sealing of the wide-mouth bottles of a brown color, as this is a crucial step in preventing the volatilization of DCM.

The next step involves the injection of 10 mL of spinning solution into a disposable syringe. This is followed by the expulsion of the internal air and the fixation of the syringe on a constant flow injection pump. In accordance with the optimal conditions for pure PLA, it is imperative to select a spinning voltage of 20 kV and a spinning distance of 18 cm. Concurrently, the receiving plate should be configured as a 20 × 20 cm aluminum foil paper. The spinning speed is set at 1 mL per hour, the ambient temperature is maintained at 25 ±1 °C, the humidity level is controlled to 55 ±1%, and specific shading treatments are implemented to avert DCM from undergoing photocatalysis during the spinning process.

Performance characterization

The nanofiber membrane was then exposed to a surface spray gold treatment. The fiber morphology was observed using SEM. The cold field acceleration voltage was set to 3 kV or 5 kV (adjusted according to clarity), and SEM images at different magnifications (2000, 5000, 10000, 20000, *etc.*) were taken and saved for later use. A sample size of $n = 100$ fibers was randomly selected from numerous electron microscope images for backup. The selected fibers must originate from disparate regions and be subjected to extensive magnification. The fiber diameter was measured using IMAGEJ software, and the probability distribution of fiber diameter was analyzed using Origin software. A corresponding Gaussian distribution curve was plotted, and the mean value, standard deviation, and confidence interval of the fiber diameter were calculated.

In order to investigate the thermal performance changes of nanofiber membranes with different GO contents, a synchronous thermal analyzer (TG/DTA5700) was used to analyze the thermal stability of the membranes. The membranes were then dried, pulverized, and examined using a synchronous thermal analyzer within an inert gas, N_2, environment. The flow rate was set at 50 mL per minute, the temperature range was set from 30 °C to 600 °C, and the heating rate was set at 10 °C per minute. The slow heating rate can ensure more complete thermal decomposition, and it is important to note that the mass of the membrane added should be between 5 mL and 10 mL.

Results and analysis

The SEM images and diameter distribution of the PLA fiber membranes prepared by the orthogonal method are shown in fig. 1, where figs. 1(a)-1(i) correspond to experiments 1-9 in tab. 4. A thorough examination of the SEM images in figs. 1(a)-1(i) reveals that the fiber morphology exhibits variation in response to varying solvent ratios (DCM:DMF). When the DCM:DMF ratio is set to 7:3, as illustrated in figs. 1(a), 1(d), and 1(g), the fiber surface exhibits a lack of smoothness, accompanied by the formation of wrinkles. As the concentration of PLA is reduced, the visibility of the wrinkles increases. The image illustrates the most prominent wrinkles. When the DCM:DMF ratio is set to 8:2, as illustrated in figs. 1(b), 1(e), and 1(h), a substantial number of longitudinal cracks emerge on the fiber surface, and certain fibers begin to manifest porous structures.

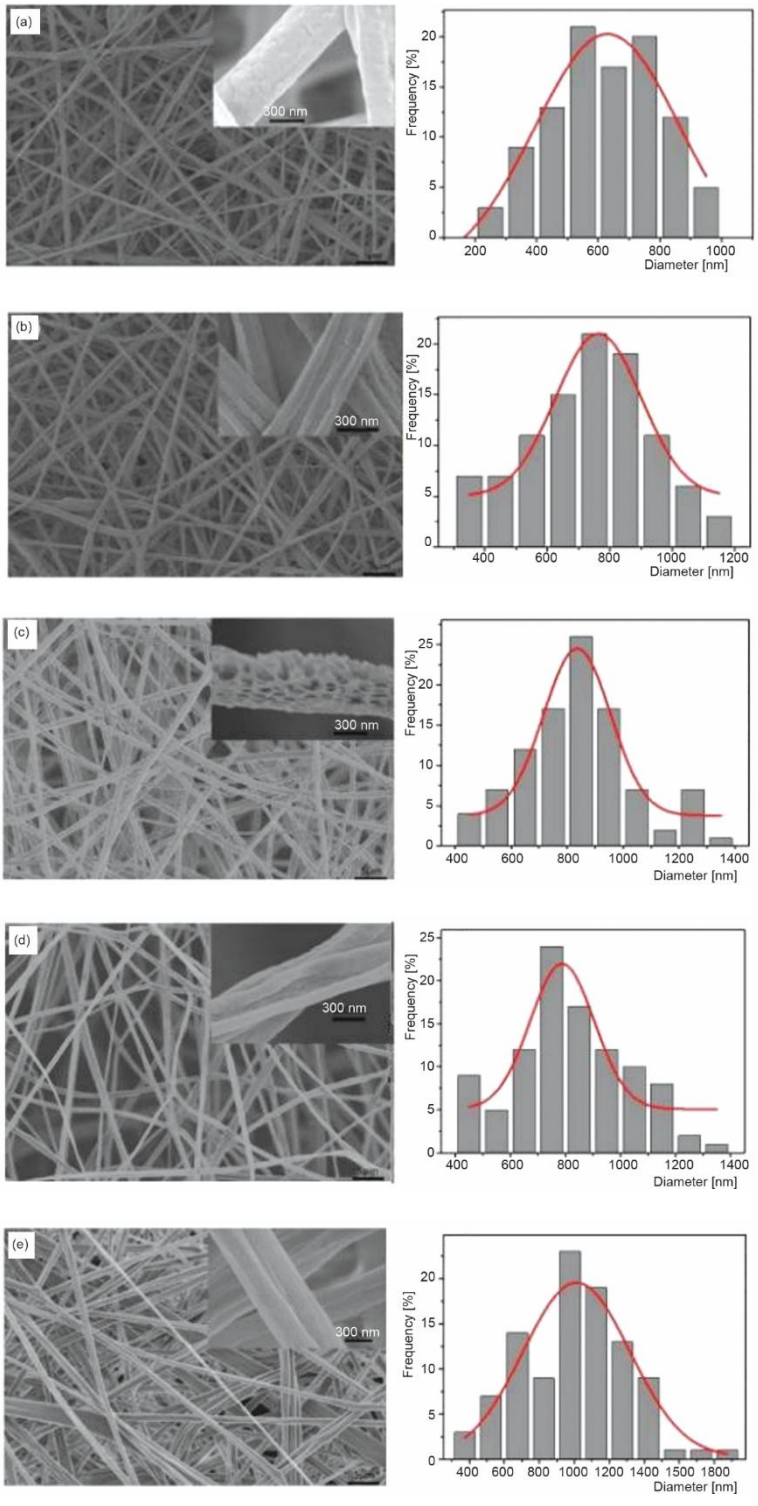
(a)
300 nm
Frequency [%]
Diameter [nm]
(b)
300 nm
Frequency [%]
Diameter [nm]
(c)
300 nm
Frequency [%]
Diameter [nm]
(d)
300 nm
Frequency [%]
Diameter [nm]
(e)
300 nm
Frequency [%]
Diameter [nm]

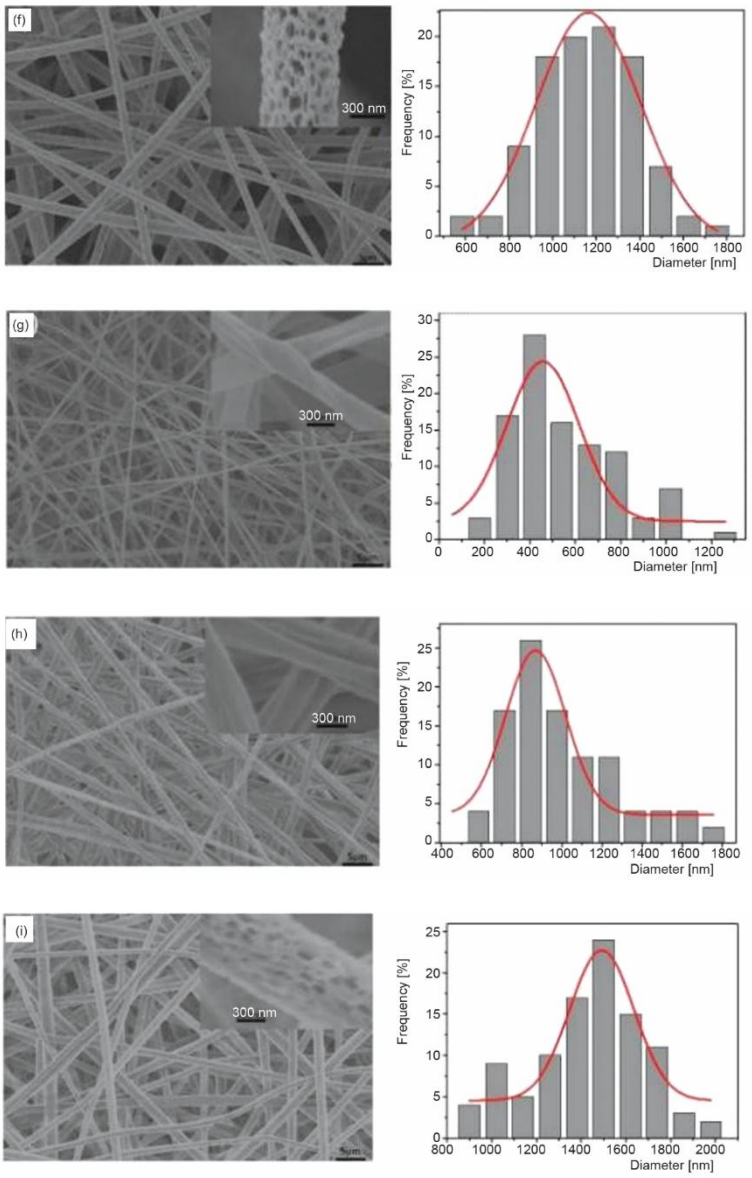

Figure 1. The SEM images and diameter distribution of PLA fiber membrane prepared by orthogonal method, (a)-(i) correspond to Nos. 1-9 test in tab. 5, respectively

However, these pores are minute and irregular in shape. When the DCM:DMF ratio is set at 9:1, as illustrated in figs. 1(c), 1(f), and 1(i), the fiber surface displays a distributed porous structure, with a uniform distribution. Figure 1(c) offers the most evident illustration of this porous structure distribution. It has been demonstrated that a decrease in the concentration of PLA results in an increase in the fineness of the fibers and the density of the pore distribution.

The mean diameter data of the fibers are documented in tab. 5, and their confidence intervals are calculated using eq. (1). Experiment 5 exhibited the most extensive confidence interval, and fig. 1(e) also demonstrated the most uneven fiber thickness. This finding offers an indirect indication that when the fibers are on the verge of exhibiting porous structures, they are susceptible to uneven thickness between individual fibers. Conversely, experiments 1, 2, and 3 exhibited relatively narrow confidence intervals, suggesting that the fibers produced exhibited enhanced uniformity.

$$\text{Confidence level} = \frac{1.96\sigma}{\sqrt{n}} \tag{3}$$

where σ is the standard deviation, n – the sample size is 100 fibers, 1.96 – the confidence constant at 95%.

Table 4. Experimental results and visual analysis

Test number	PLA solute concentration [wt.%] - A	Solvent ratio (DMC:DMF) - B	Spinning voltage [kV] - C	Spinning receiving distance [cm] - D	Average diameter [nm]
1	1	1	1	1	620
2	1	2	2	2	741
3	1	3	3	3	846
4	2	1	2	3	820
5	2	2	3	1	978
6	2	3	1	2	1152
7	3	1	3	2	555
8	3	2	1	3	1001
9	3	3	2	1	1437
K_1	2207	1995	2773	3035	
K_2	2950	2720	2998	2448	
K_3	2993	3435	2379	2667	
k_1	736	665	924	1012	T = 8150
k_2	983	907	999	816	
k_3	998	1145	793	889	
R	262	480	206	196	

Table 5. Average diameter and standard deviation of PLA fiber prepared by orthogonal test

Test number	1	2	3	4	5	6	7	8	9
Standard deviation σ [nm]	177	197	195	205	299	222	223	276	248
Confidence interval [nm]	±34.6	±38.6	±38.2	±40.1	±58.6	±43.5	±43.7	±54.1	±48.6

It should be noted that K_i in tab. 4 represents the sum of the experimental results corresponding to the factor at level *i*. Furthermore, K_i is the average value of the experimental results corresponding to the factor at level *i*. Finally, $R = K_{i.\max}\ k_{i.\min}$, and *T* represents the sum of the average diameters under all tests.

As illustrated in tab. 4, the sequence is RB > RA > RC > RD. In the PLA nanofiber spinning process, the solvent ratio (DCM:DMF) has the most significant impact on fiber diameter, followed by the concentration of the PLA solute and the spinning voltage. The influence of spinning receiving distance on fiber diameter is the least significant. As illustrated in tab. 4, it is evident that KA1 is less than KA2 and KA3, KB1 is less than KB2 and KB3, and KC3 is less than KC1 and KC2. Additionally, KD2 is less than KD3 and KD1. As illustrated in fig. 1(a), the solute concentration exerts a significant influence on fiber diameter. An examination of the trend chart reveals a substantial correlation between solute concentration and fiber diameter. Constant other factors being assumed, an increase in fiber diameter is observed with an increase in concentration. Upon attaining a specified solute concentration, the increase becomes more gradual. This phenomenon is attributed to the increase in polymer content, which leads to an increase in solution viscosity and a decrease in the amount of volatile solvent. The result of these changes is an increase in fiber diameter. Consequently, to produce nanofibers with enhanced porosity, it is recommended to employ a PLA solution with a concentration of 8 wt.%. As illustrated in fig. 1(b), the solvent ratio exerts a significant influence on fiber diameter. An examination of the trend chart reveals a substantial influence of the solvent ratio on fiber diameter. The distribution depicted in the graph bears a strong resemblance to a linear function distribution. The DCM is a volatile solvent, and as the amount of dichloromethane increases, the fiber diameter also increases. Given the objective of this study, which is to prepare porous nanofibers, and in consideration of the solvent ratio commonly employed in the extant literature, which is 9:1, it can be concluded that a solvent ratio of DCM:DMF = 9:1 is more suitable. Figure 1(c) illustrates the impact of varying the spinning voltage on the mean diameter of the fibers. When the spinning voltage is ≤ 18 kV, the average diameter of the fibers is larger, exceeding 900 nm. It is imperative to acknowledge that the impact of spinning voltage on fiber diameter is considerably less pronounced in comparison to solute concentration and solvent ratio. To ensure the fabrication of more stable and finer porous nanofibers, it is recommended to employ a spinning voltage of 20 kV. Figure 1(d) illustrates the impact of varying spinning distance on fiber diameter. This factor is of minimal importance. As the spinning distance increases, the average diameter of the fibers initially decreases and then exhibits a slight increase. When the distance between the receiving plate and the injector needle is minimal, at 15 cm, the spinning voltage does not have sufficient time to stretch and thin the spinning solution, resulting in a larger fiber diameter. When the receiving plate is at a greater distance, specifically 21 cm, the volatile solvent undergoes more complete evaporation during the spinning process. This increased evaporation leads to an augmentation in the fiber diameter to a certain extent. A receiving distance of 18 cm is deemed more suitable when taking into account both porosity and fineness factors.

According to the results of the orthogonal experiment, the optimal process conditions for preparing PLA porous nanofibers are: It is evident that $A_1B_3C_3D_2$ signifies that the solute concentration of the spinning solution is 8 wt.%, the solvent ratio (DCM:DMF) is 9:1, the spinning voltage is 20 kV, and the spinning distance is 18 cm.

The morphology of the fibers was observed using SEM after the PLA/GO porous nanofibers, prepared by electrospinning, were spray-coated with gold. The electron microsco-

py images and diameter analysis are shown in fig. 2. The mean diameter, standard deviation, and confidence interval of the fibers are presented in tab. 6.

Table 6. Average diameter and standard deviation of porous nanofibers with different GO contents

Serial number	GO concentration [wt.%]	Average diameter [nm]	Standard deviation σ [nm]	Confidence interval [nm]
1	0	846	195	±38.2
2	0.1	893	149	±29.3
3	0.2	633	140	±27.5
4	0.5	617	103	±20.3
5	1.0	865	269	±52.6

Figure 2 presents the SEM images and diameter distribution of porous nanofibers with varying GO contents, which can be analyzed based on the data presented in tab. 6. As illustrated in fig. 2(a), with a GO content of 0.1 wt.%, the average diameter of the fibers exhibited a modest increase of 5.6% compared to the pure PLA porous nanofibers. However, the standard deviation decreased by 23.6%, indicative of enhanced uniformity in the fiber diameter. As illustrated in fig. 2(b), the average diameter of the fibers decreased by 25.2% compared to PLA porous nanofibers, with a GO content of 0.2 wt.%. The standard deviation also exhibited a decrease of 28.2%, demonstrating a comparable reduction to that observed with the 0.1 wt.% GO content. As illustrated in fig. 2(c), at a GO content of 0.5 wt.%, the average fiber diameter attained a minimum value across the range of GO contents, exhibiting a 27.1% reduction compared to PLA porous nanofibers. The thickness of the fibers was found to be analogous to that of the 0.2 wt.% GO content. However, a significant decrease of 47.2% in the standard deviation was observed, suggesting a more uniform fiber diameter, as evidenced by the SEM image. As illustrated in figs. 2(a)-2(c), it can be discerned that an augmentation in the GO content results in an escalation in the conductivity of the spinning solution. Additionally, the charge carried by the jet on the surface of the polymer during the spinning process also increases. The application of an electric field force facilitates the elongation and stretching of the spinning solution, thereby reducing the average fiber diameter and enhancing the uniformity of thickness. The increase in fiber diameter by 5.6% in fig. 2(a) may be attributed to the inadequate effect of the low GO content on the spinning process, resulting in fluctuations in the fiber diameter within a certain range. The content of GO in fig. 2(d) is 1.0 wt.%, and the average diameter of the fiber becomes similar to that of the PLA porous fiber. Concurrently, the fiber's thickness exhibited unevenness, with a standard deviation that increased by 37.9%. As the go content increases, the viscosity of the spinning solution rises, the repulsion of the polymer macromolecular chain in the electric field increases, and the *whipping* state of the jet is inhibited to a certain extent, thereby increasing the average diameter of the fiber. The fiber exhibits variability in thickness to a certain extent.

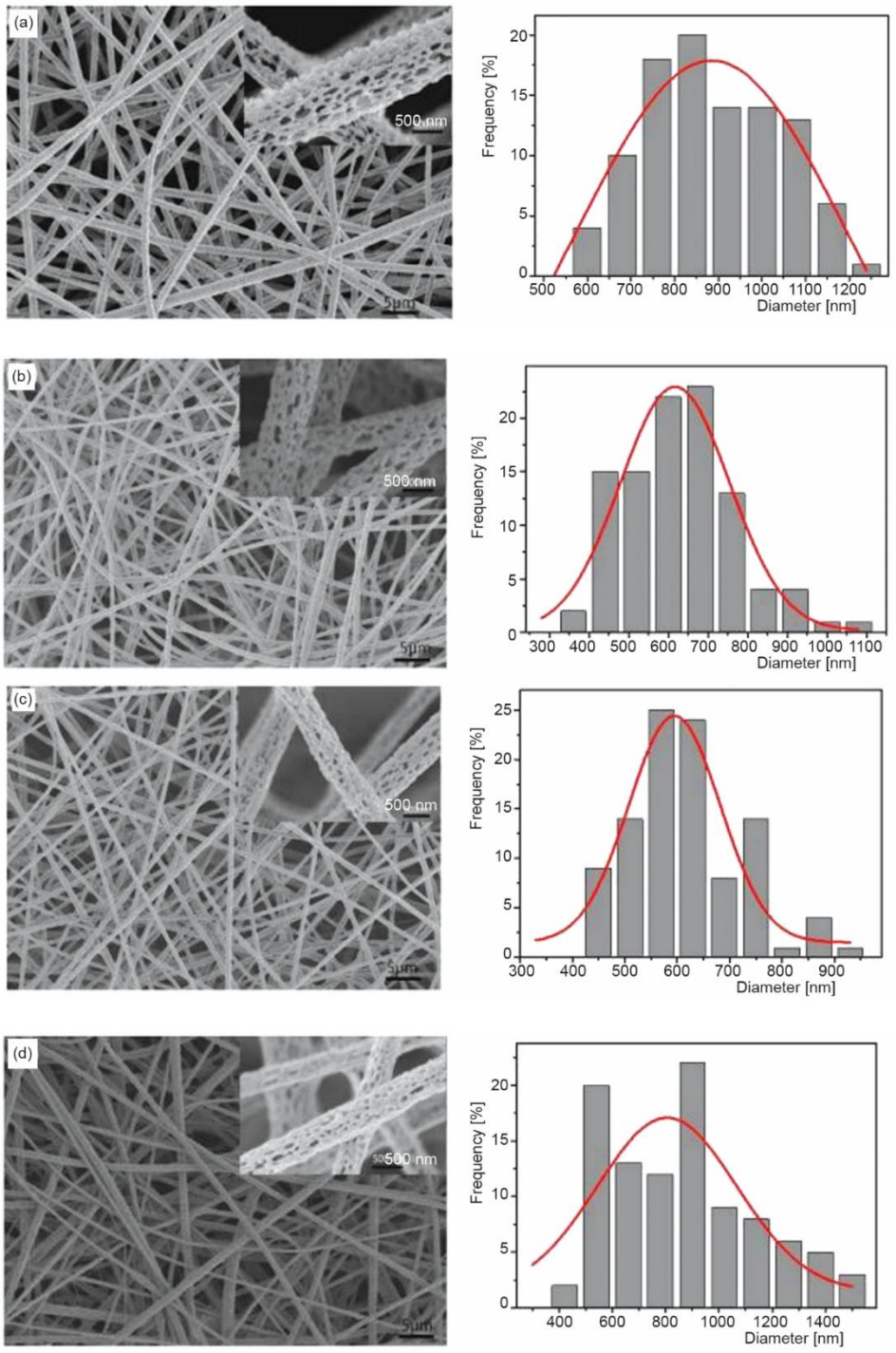

Figure 2. The SEM images and diameter distribution of porous nanofibers with different GO contents

The thermogravimetric (TG) and derivative thermogravimetric (DTG) curves of pure PLA porous nanofibers and PLA/GO nanofibers with different GO contents are shown in fig. 3. As illustrated in fig. 3, a discernible similarity is observed in the trends exhibited by their TG and DTG curves. Prior to the temperature of 150 °C, all specimens exhibited a certain degree of mass loss, accompanied by fluctuations, which can be attributed to the volatilization of residual moisture and solvents present within the fibers. The relevant data are documented in tab. 7. It has been observed that pure PLA leaves only 0.002% residue after thermal decomposition, indicating that almost no residual substances are present. The onset degradation temperature has been determined to be 291.64 °C. However, when GO is incorporated into pure PLA porous fibers, the amount of residue after thermal decomposition significantly increases, and the onset degradation temperature is slightly higher, approximately 25-30 °C. All samples exhibited maximum mass loss at approximately 362 °C, with the process halting at 382 °C, resulting in complete combustion of the fibers. The GO is known

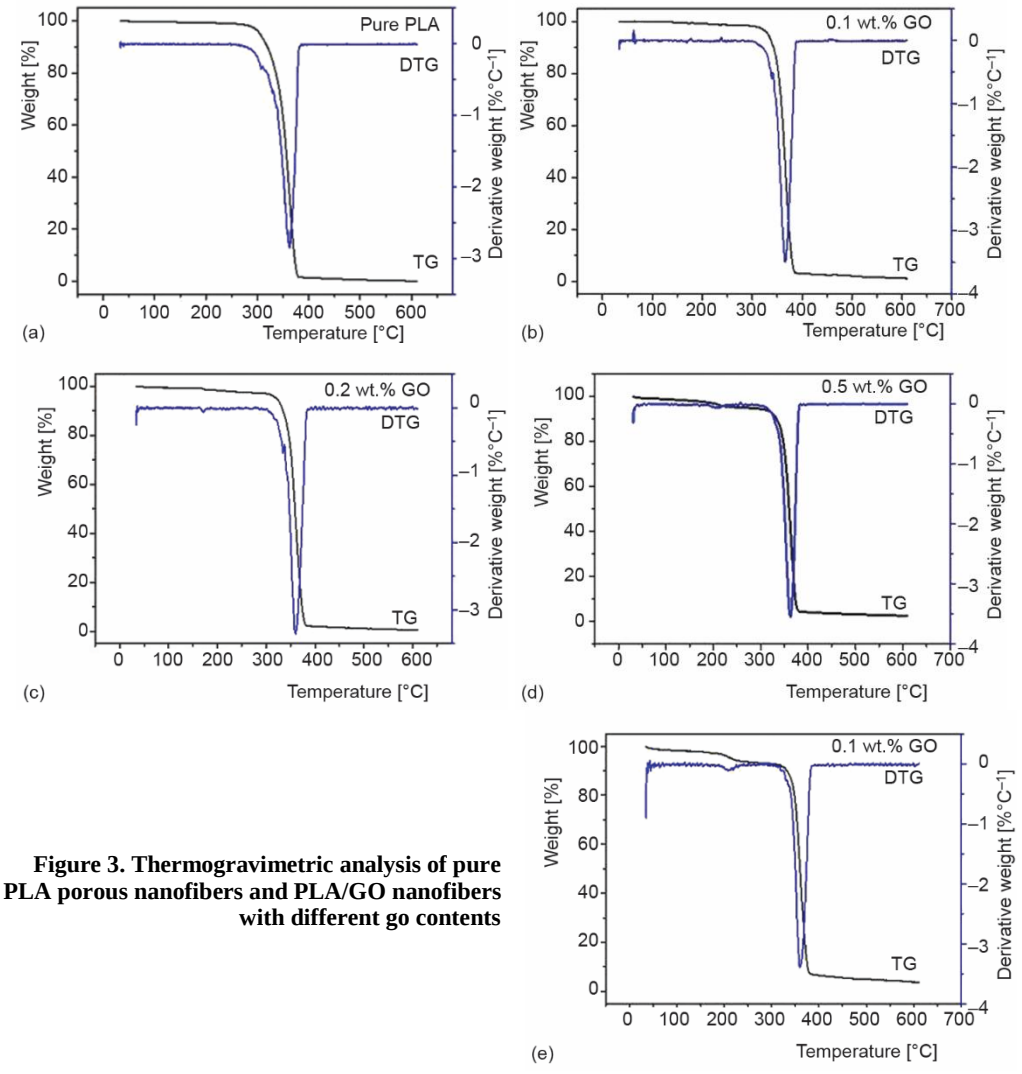

Figure 3. Thermogravimetric analysis of pure PLA porous nanofibers and PLA/GO nanofibers with different go contents

to be thermally unstable when exposed to nitrogen. When heated to approximately 500 °C, the oxidation functional groups of GO decompose, resulting in a weight loss of approximately 40%-50%. However, all the hybrid materials demonstrate superior thermal stability post-decomposition, persisting only beyond 600 °C. Consequently, the incorporation of GO leads to a substantial augmentation in the residual mass fraction of the fibers. When GO = 0.5 wt.%, the residual mass is 2.625%.

Table 7. Thermogravimetric data of pure PLA porous nanofibers and PLA/GO porous nanofibers with different go contents

Number	GO concentration [wt.%]	Fiber weight [mg]	Residual mass percentage [%]	Starting temperature of TG curve [°C]	Peak temperature of DTG curve [°C]	Endpoint temperature of TG curve [°C]
1	0	5.34	0.002%	291.65	361.39	380.65
2	0.1	5.53	1.076%	319.59	365.99	386.63
3	0.2	6.74	1.135%	314.71	366.51	382.33
4	0.5	5.76	2.625%	317.49	362.67	380.49
5	1.0	5.85	3.674%	318.27	361.41	383.03

Conclusions

In summary, this study optimized the preparation of PLA porous nanofibers through the implementation of orthogonal experiments, thereby identifying the optimal process parameters. These parameters include an 8 wt.% PLA solute concentration, a DCM:DMF solvent ratio of 9:1, a 20 kV spinning voltage, and a 18 cm spinning distance.

With regard to the application of bubble electrospinning [18-20], although not directly examined in this study, its potential merits further exploration. Given the efficacy of electrospinning in the preparation of porous nanofibers, the application of bubble electrospinning, a variation of electrospinning, may offer unique advantages. This approach has the potential to yield more complex pore structures or enhance the porosity to a greater extent, thereby opening new avenues for the development of high-performance nanofiber membranes in the future.

Acknowledgment

Jiangming Wang and Lei Zhao are co-first authors of this article. This work is supported by Provincial Scientific Research Platform Open Project Funding of Yancheng Polytechnic College (YGKF202011). The work is also funded by Qing Lan Project of Jiangsu Colleges and Universities for Excellent Teaching Team in 2023, Letter from the Faculty Department of Jiangsu Provincial Department of Education (2023) No. 27, the doctoral research initiation fund project of Yancheng Polytechnic College (2023), Jiangsu Province Higher Vocational Education High-level Major Group Construction Project-Modern Textile Technology Major Group (Grant number: Jiangsu Vocational Education 2020. No 31). Brand Major Construction Project of International Talent Training in Colleges and Universities-Modern Textile Technology Major (Grant number: Jiangsu Foreign Cooperation Exchange Education 2022. No 8) also supports the research of this subject. Key technology innovation platform for flame retardant fiber and functional textiles in Jiangsu Province (2022JMRH-003) also supports this research.

References

[1] Zhao, L., *et al.*, A Spider-Inspired Electrospinning for Fabrication of Polyvinylidene Fluoride Nanofiber Membranes, *Thermal Science*, *28* (2024), 3A, pp. 2251-2258
[2] Xu, Z. Z., *et al.*, Biomimetic Microspheres with Rough Structure by the Geometric Potential Theory, *Thermal Science*, *28* (2024), 3A, pp. 2269-2275
[3] Wei, L., *et al.*, The Bubble Electrostatic Spraying: A New Technology for Fabrication of Superhydrophobic Nanofiber Membranes, *Thermal Science*, *28* (2024), 3A, pp. 2259-2267
[4] Liu, H. Y., *et al.*, Interaction of Multiple Jets in Bubble Electrospinning, *Thermal Science*, *27* (2023), 3A, pp. 1741-1746
[5] Zhou, H., Lee, J., Nanoscale Hydroxyapatite Particles for Bone Tissue Engineering, *Acta Biomaterialia*, *7* (2011), 7, pp. 2769-2781
[6] Yuan, S., *et al.*, Stable Metal-Organic Frameworks: Design, Synthesis, and Applications, *Advanced Materials*, *30* (2018), 1704303
[7] Li, Q., *et al.*, Fabrication of Porous TiO_2 Nanofiber and its Photocatalytic Activity, *Materials Research Bulletin*, *46* (2011), 11, pp. 2094-2099
[8] Li, X. X., *et al.*, Elucidating the Fractal Nature of the Porosity of Nanofiber Members in the Electrospinning Process, *Fractals*, *32* (2024), 2450109
[9] Liang, Y, *et al.*, Silver Nanoparticle-Immobilized Porous POM/PLLA Nanofibrous Membranes: Efficient Catalysts for Reduction of 4-Nitroaniline, *RSC Advances*, *7* (2017), 13, pp. 7460-7468
[10] He, C.-H. A Variational Principle for a Fractal Nano/Microelectromechanical (N/MEMS) System, *Int. J. Numer. Method. H.*, *33* (2023), 1, pp. 351-359
[11] He, J.-H, *et al.*, Modeling and Numerical Analysis for an MEMS Graphene Resonator, *Front. Phys. 13* (2025), 1551969
[12] He, J.-H. Periodic Solution of a Micro-Electromechanical System, *Facta Universitatis, Series: Mechanical Engineering, 22* (2024), 2, pp. 187-198
[13] Lerf, A., *et al.*, Hydration Behavior and Dynamics of Water Molecules in Graphite Oxide, *Journal of Physics and Chemistry of Solids*, *67* (2006), 5-6, pp. 1106-1110
[14] Wu, S, *et al.*, Surface Modified Electrospun Porous Magnetic Hollow Fibers Using Secondary Downstream Collection Solvent Contouring, *Materials Letters*, *204* (2017), Oct., pp. 73-76
[15] Feng, W, *et al.*, Well-Aligned Polyaniline/Carbon-Nanotube Composite Films Grown by In-Situ Aniline Polymerization, *Carbon*, *41* (2003), 8, pp. 1551-1557
[16] Zhu, J, *et al.*, Electrospinning Poly (L-Lactic Acid) Piezoelectric Ordered Porous Nanofibers for Strain Sensing and Energy Harvesting, *Journal of Materials Science: Materials in Electronics*, *28* (2017), 16, pp. 12080-12085
[17] He, C.-H. *et al.*, Taylor Series Solution for Fractal Bratu-Type Equation Arising in Electrospinning Process, *Fractals*, *28* (2020), 2050011
[18] He, J.-H., *et al.*, The Maximal Wrinkle Angle During the Bubble Collapse and Its Application to the Bubble Electrospinning, *Frontiers in Materials*, *8* (2022), 800567
[19] Qian, M. Y., He, J.-H., Collection of Polymer Bubble as a Nanoscale Membrane, *Surfaces and Interface*, *28* (2022), 101665
[20] Ali, M., *et al.*, Double Bubble Electrospinning: Patents and Nanoscale Interface, *Recent Patents on Nanotechnology 19* (2024), 3, pp. 453-465

Paper submitted: October 10, 2024
Paper revised: May 9, 2025
Paper accepted: May 23, 2025